Applied Catalysis B: Environmental 191 (2016) 202–208

Contents lists available at ScienceDirect

Applied Catalysis B: Environmental

journal homepage: www.elsevier.com/locate/apcatb

Nitrogen-doped hollow carbon spheres with highly graphitized mesoporous shell: Role of Fe for oxygen evolution reaction

Min Young Song[a,b], Dae-Soo Yang[a,b], Kiran Pal Singh[a], Jinliang Yuan[c], Jong-Sung Yu[a,*]

[a] Department of Energy System Engineering, DGIST, Daegu 42988, Republic of Korea
[b] Department of Advanced Materials Chemistry, Korea University, 2511 Sejong-ro, Sejong 339-700, Republic of Korea
[c] Department of Energy Sciences, Faculty of Engineering, Lund University, Box 118, 22100, Lund, Sweden

ARTICLE INFO

Article history:
Received 27 November 2015
Received in revised form 1 March 2016
Accepted 15 March 2016
Available online 16 March 2016

Keywords:
Hollow carbon
Graphitized carbon
Nitrogen-doped
Iron
Oxygen evolution reaction

ABSTRACT

There are many studies portraying iron (Fe) and nitrogen (N)-functionalzed carbon as an electrocatalyst along with possible elucidation of catalytically active sites. Despite continuous controversial debate on the active sites/species, the presence of N is believed to be undeniably needed for the efficient catalysis, whereas the necessity and role of Fe are still debated. To clearly understand the role of Fe in Fe and N-functionalized electrocatalyst, N-doped hollow mesoporous shell carbon (N-HMSC) is prepared as a uniform model electrocatalyst by a simple template nanocasting using Fe phthalocyanine (FePc) as a single precursor for carbon, N, and Fe. It is found that the presence of Fe in N-HMSC leads to the efficient graphitization of N-HMSC structure, which can be beneficial for electrocatalytic oxygen evolution reaction (OER). Interestingly, it is observed that Fe is a must for the preparation of high efficient catalyst, but may not be necessary for OER.

1. Introduction

There is a growing interest in search for new catalysts to enhance the activity and kinetics of oxygen evolution reaction (OER) as well as oxygen reduction reaction (ORR). The OER ($4OH^- \rightarrow 2H_2O + 4e^- + O_2$ in alkaline medium) plays pivotal roles in various renewable energy conversion and storage technologies, such as solar cell, Li-air batteries, and hydrogen generation from water splitting [1–5]. Up to now, Ru and Ir metals and oxides have shown the best OER performance, but their high cost and poor durability severely hinder their commercial applicability [6–9]. Therefore, it is highly desirable to develop an efficient and low-cost OER catalyst to replace the precious metal-based catalysts. Recently, extensive efforts have been made towards finding efficient and low-cost OER catalysts, among which perovskites [10] and transition metal-based non-precious metal catalysts [11–16] have shown some promising results.

It has been also reported that heteroatom doping into carbon matrix can significantly change the electronic properties of carbon along with its favorable chemical response towards OER as well as ORR [17–21]. Qiao and co-workers reported 3D electrode composed of N and O duel-doped graphene-CNT hydrogel film as a high efficient electrode for OER [20]. Even though resulting doped catalyst possesses the low cost and excellent durability, the catalytic activity towards OER and ORR is found to be still not much promising [22,23]. Therefore, the heteroatom-doped carbon study was further extended to metal-coordinated heteroatom-doped carbon. It was found that metal coordination to heteroatom-doped carbon can further enhance the electrocatalytic activity of the doped carbon, particularly in ORR due to the formation of active metal-heteroatom species [24–28]. However, studies on metal/heteroatom-doped carbon for OER are still very limited [4,29–35]. Lu et al. reported Fe-N-carbon sheets to load NiO particles for synergistic OER catalysis [13]. Recently, Zhao et al. demonstrated Fe/N-carbon-based materials as bi-functional catalysts for ORR and OER [17,31]. However, there have been continued controversial debates on the active sites in M-N-C catalytic materials. The role of Fe in the electrocatalytic ORR and OER still remains vague and should be seriously considered to explore the full potential of Fe/N-based carbon catalyst.

Recently, several works reported the ORR performance of non-precious metal coordinated to heteroatom-doped hierarchical porous carbon [36,37]. Zhou et al. reported Fe/N-doped hollow core shell carbon for efficient ORR catalyst in acid media [38]. However, there is no discussion on the role and necessity of the Fe considered to be coordinated to N doped in carbon for enhancing the electrocatalytic ORR activity. Recently, Yu and co-workers have tried to address the role of Fe species in the formation of an efficient catalyst by comparing the ORR activity of Fe/N-doped and N-doped carbons [39]. However, to the best of knowledge, there has been no report

* Corresponding author.
E-mail address: jsyu@dgist.ac.kr (J.-S. Yu).

http://dx.doi.org/10.1016/j.apcatb.2016.03.031
0926-3373/

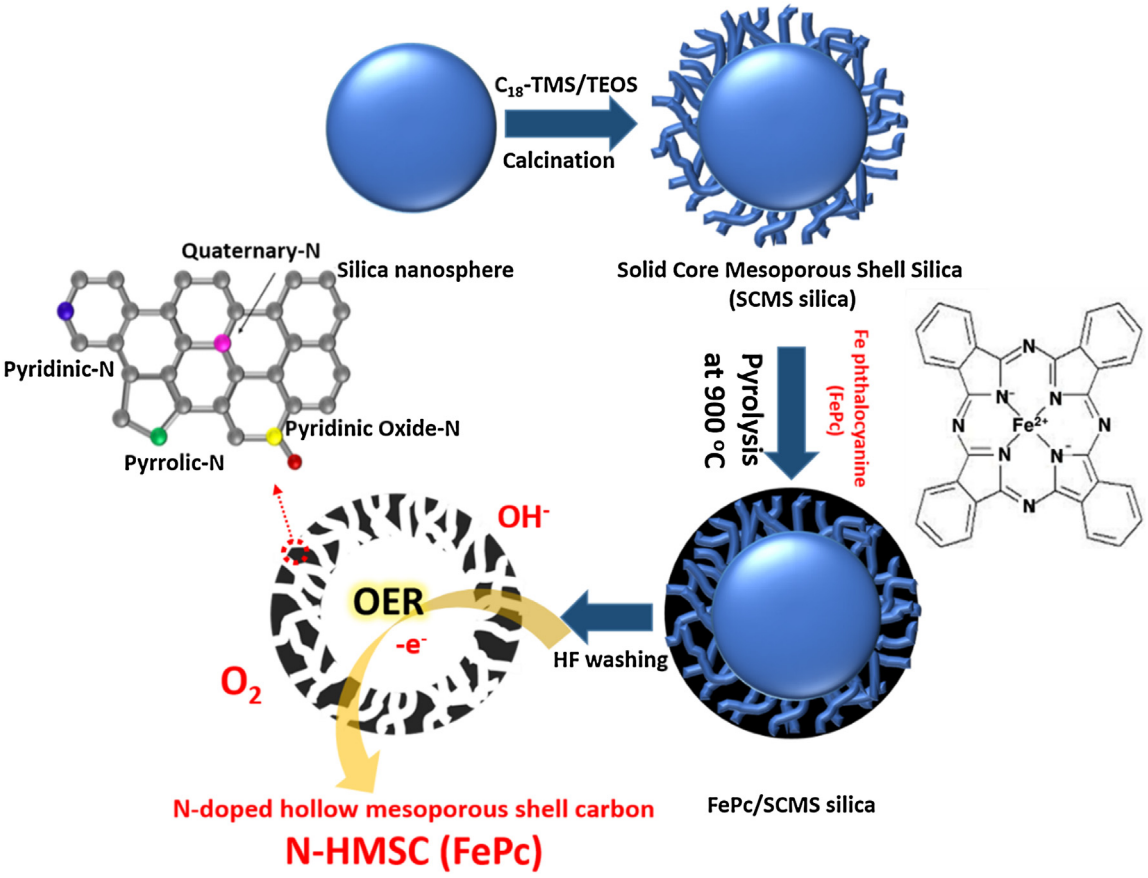

Scheme 1. Schematic illustration of synthesis route to N-HMSC (FePc) and its electrocatalytic oxygen evolution reaction.

describing the role and necessity of Fe in Fe-functionalized N-doped carbon for OER. Therefore, in this study, to understand the role of Fe and N species, presumably suggested as active species, unique Fe and N-functionalized core-shell carbon nanostructure with hollow mesoporous shell structure is synthesized as a well-defined uniform model system by nanocasting method (See Scheme 1 and experimental section). Briefly, Fe phthalocyanine (FePc) as a single precursor for C, N and Fe sources was nanocasted into the solid core mesoporous shell (SCMS) silica template followed by a one-step pyrolysis. After the pyrolysis, N-doped hollow mesoporous shell carbon (N-HMSC (FePc)) was generated by removal of the SCMS silica template using HF etching. The present route allows simultaneous introduction of N and Fe into the porous carbon structure to generate Fe and N-functionalized HMSC (FePc). Interestingly, however, it is found that HF treatment removes the Fe species as well as the silica template and eventually results in Fe-free N-doped HMSC (N-HMSC (FePc)). Hence, to selectively remove silica only, here we have treated the same as-prepared carbon/SCMS silica composite with NaOH to get Fe-functionalized N-HMSC (FePc) termed as Fe/N-HMSC (FePc). For comparison, only N-doped HMSC, i.e., N-HMSC (Pc), was also prepared using Fe-free phthalocyanine (Pc) (29H, 31H-Phthalocyanine) as N and C precursor, and un-doped HMSC, using phenol-formaldehyde polymer as C source [40]. The resulting hollow carbon materials possess high surface area as well as excellent structural uniformity. It is a general consensus that surface area and conductivity along with catalytically active center play dominating role in electrocatalysis [41]. Higher surface area can increase availability of active sites, mass transfer capability, and wetting of the carbon electrode, whereas conductivity helps in improving the electron/charge transport through the carbon surface [42]. In this respect, our high surface area uniform HMSC structure is a good choice for high electrocatalytic activity and as a model system for study of the effect of Fe on the catalyst preparation and electrocatalytic OER activity without other structural variation disturbance.

2. Experimental

2.1. Preparation of solid core mesoporous shell (SCMS) silica spheres

SCMS silica was used as a template for the synthesis of hollow mesoporous shell carbon (HMSC), N-HMSC and Fe/N-HMSC spheres [40]. A typical synthesis route for SCMS silica spheres is as follows. 40 mL of aqueous ammonia (28 wt.%) was mixed with 1.0 L of ethanol and 80 mL of deionized water. After stirring for about 15 min, 60 mL of TEOS (98%, ACROS) was added, and the reaction mixture was further stirred for 6 h to yield uniform silica spheres (Stöber silica solution). A solution containing a mixture of 35.5 mL of TEOS and 14.5 mL of C_{18}-TMS (90% tech., Aldrich) was added to the prepared colloidal solution containing the silica spheres and further reacted for 6 h. The resulting octadecyl group-incorporated mesoporous silica shell/solid core nanocomposite spheres were retrieved by centrifugation, dried at room temperature and further calcined at 550 °C for 6 h under oxygen atmosphere to remove octadecyl group in the composite and to generate the final uniform spherical SCMS silica particles (Kaiser Approach).

2.2. Preparation of hollow mesoporous shell carbon (HMSC) spheres

A typical synthesis route for HMSC spheres is as follows. 0.374 g of phenol and 0.238 g of paraformaldehyde per gram of the SCMS

silica template were incorporated into the mesopores of the SCMS silica by heating the reaction mixture at 180 °C for 12 h under static vacuum to yield phenol-resin/SCMS silica composite. The composite was carbonized at 900 °C for 3 h under argon atmosphere to carbonize the phenol resin inside the mesopores of SCMS silica and finally to obtain carbon/silica composite. The dissolution of the SCMS silica template using HF in a 1:1 mixture of H_2O generated silica-free HMSC spheres.

2.3. Preparation of N-HMSC (Pc) or N-HMSC (FePc)

N-HMSC (Pc) or N-HMSC (FePc) spheres were synthesized through the same nanocasting as mentioned above using phthalocyanine (Pc) or Fe phthalocyanine (FePc) instead of paraformaldehyde as carbon precursor. A typical synthesis route for N-HMSC (Pc) and N-HMSC (FePc) spheres is as follows. A total of 0.5 g of SCMS silica was added to a solution containing 0.5 g of Pc or FePc in 10 mL of Ethanol, and the resulting solution was induced to be incorporated into the mesopores of SCMS silica template under static vacuum. The powder was dried at room temperature and further carbonized at 900 °C for 3 h under argon atmosphere. The resulting black powder composite was then stirred in an aqueous HF solution (HF: deionized H_2O = 1:1) for 24 h at room temperature, and product was copiously washed with water. Afterwards, the material was dried at 80 °C in an oven to have N-HMSC (Pc) or N-HMSC (FePc) samples. In another series of experiment with FePc, the black calcined powder composite was stirred in 2.0 M NaOH solution instead of HF for 24 h at room temperature to selectively dissolve SCMS silica template alone to produce Fe/N-HMSC (FePc) spheres.

2.4. Instrumental analysis

The morphology and microstructure of the obtained samples were investigated by scanning electron microscopy (SEM) analysis with a Hitachi (S-4700, Hitachi, Japan) microscope operated at acceleration voltage of 10 kV. Transmission electron microscopy (TEM) was operated at 120 kV with EM912 Omega. High-resolution TEM (HR-TEM) images were obtained by using JEOL FE-2010 microscope operated at 200 kV. The purity of the samples was examined by X-ray diffraction (XRD) analysis with a Rigaku Smartlab X-ray diffractometer with Cu Kα radiation (λ=1.5406 Å) operated at 40 kV and 30 mA. The average lattice spacing size (d) of the samples was estimated by applying Scherer formula: $d = n\lambda/2\sin\theta$, where λ is the X-ray wavelength, n is a Scherer constant, which is taken as 0.89, and θ is the Bragg diffraction angle. X-ray photoelectron spectroscopy (XPS) analyses were carried out with an ESCALAB 250 XPS System using a monochromated Al Kα (150 W) source. The nitrogen adsorption-desorption isotherms were measured at −196 °C using a Micrometrics ASAP 2020 accelerated surface area and porosimetry system. Specific surface areas of the samples were determined by nitrogen adsorption data in the relative pressure range from 0.05 to 0.2 using the Brunauer–Emmett–Teller (BET) equation. Total pore volume was determined from the amount of gas adsorbed at the relative pressure of 0.99. Pore size distribution (PSD) was calculated from the adsorption branches by the Barrett–Joyner–Halenda (BJH) method. Raman spectra were recorded with a Renishaw spectrometer using an Ar ion laser (λ = 514.5 nm).

2.5. Electrode preparation and electrochemical characterization

The working electrode was polished with alumina slurry to obtain a mirror-like surface, then washed with Mill-Q water and acetone, and dried before use. The slurry was prepared by mixing 5.0 mg of catalysts added into a 1.0 mL solvent mixture of Nafion (5 wt.%) and water with v/v ratio of 1:9 for 20 min in an ultrasonicator. For comparison, a commercially available catalyst of 20 wt.% Pt/C (E-TEK) was used, and a 1.0 mg/mL commercial Pt/C suspension was prepared according to the identical procedure described above. The slurry was placed on pre-cleaned working electrode, and the electrode was allowed to dry at room temperature before the measurement. This leads to catalyst loading of 0.4 μg cm^{-2} for either HCMS catalyst or commercial 20 wt.% Pt/C. The electrochemical performances of the electrodes were characterized by cyclic voltammetry (CV), linear scan voltammetry (LSV), and chronoamperometry. Electrochemical impedance spectra (EIS) were recorded in the frequency range from 100 kHz to 0.1 Hz with and AC signal amplitude of 5 mV.

The aqueous electrolyte (0.1 M KOH) used was degassed with nitrogen before the electrochemical measurements. The electrochemical studies were carried using Biologic VMP3 electrochemical workstation. For the OER test, rotating-disk electrode (RDE) was used, and the working electrode was scanned from 0 to 1.0 V (vs. Ag/AgCl) at a scan rate of 5 mV s^{-1} in a N_2-saturated electrolyte with the electrode rotating at 1600 rpm. The potentials versus Ag/AgCl reference electrode were converted to the reversible hydrogen electrode (RHE) scale via the Nernest equation;

$$E_{RHE} = E_{Ag/AgCl} + 0.0591pH + E_{\theta Ag/AgCl} \quad (1)$$

$$\eta = E_{RHE} - 1.23\,V \quad (2)$$

where E_{RHE} is the converted potential versus RHE, $E_{Ag/AgCl}$ is the experimental potential measured against the Ag/AgCl reference electrode, $E^{\theta}_{Ag/AgCl}$ is the standard potential of Ag/AgCl at 25 °C (0.205 V), and η is the overpotential. The electrochemical measurements were carried out in 0.1 M KOH (pH = 13) at room temperature: therefore, $E_{RHE} = E_{Ag/AgCl} + 0.973\,V$.

3. Results and discussion

The topological features of the prepared catalysts are evaluated using scanning electron microscopy (SEM) and transmission electron microscopy (TEM) (Fig. S1 of supplementary Information (SI)). The TEM images illustrate the unique hollow mesoporous shell structure. It can be seen that all the samples reveal core-shell spherical structures with remarkable uniformity along with narrow size distribution in hollow core diameter (250 ± 10 nm) and porous shell thickness (40 ± 10 nm). Interestingly, however, in the case of N-HMSC (FePc), the surface roughness is found to increase along with the formation of some extra structure on the shell surface (Fig. S1(c) and (f) of SI). To examine this structure in more details, high resolution-transmission electron microscopic (HR-TEM) analyses (Fig. 1(a-d)) is carried out. On a closer look, it can be seen that these extra structures formed on the surface of N-HMSC (FePc) reveal clear lattice fringes with an interplanar distance of 0.34 nm, which corresponds to the (002) plane of graphite, indicating formation of extra graphitic carbon structures on the surface. We surmise the formation of this kind of highly graphitic structure is due to the catalytic activity of Fe. The carbon precursor in vicinity of Fe gets highly graphitized and hence extrudes out on the N-HMSC (FePc) surface. However, almost all the Fe species were leached out after HF treatment, leaving behind the empty hollow graphitic carbon structures only. To justify the catalytic activity of Fe for carbon graphitization, Fe/N-HMSC (FePc) sample was produced by NaOH washing after pyrolysis of FePc/SCMS silica composite to selectively dissolve silica, and thus Fe can remain as embedded Fe particles in the Fe/ N-HMSC (FePc) framework. HR-TEM images (Fig. S3 of SI) show that graphitic phases are formed surrounding the Fe particles, clearly signifying that Fe helps to make carbon more graphitic, especially carbon in the vicinity of the Fe. This extra structures cannot be seen in HCMS and N-HCMS (Pc) samples prepared without Fe

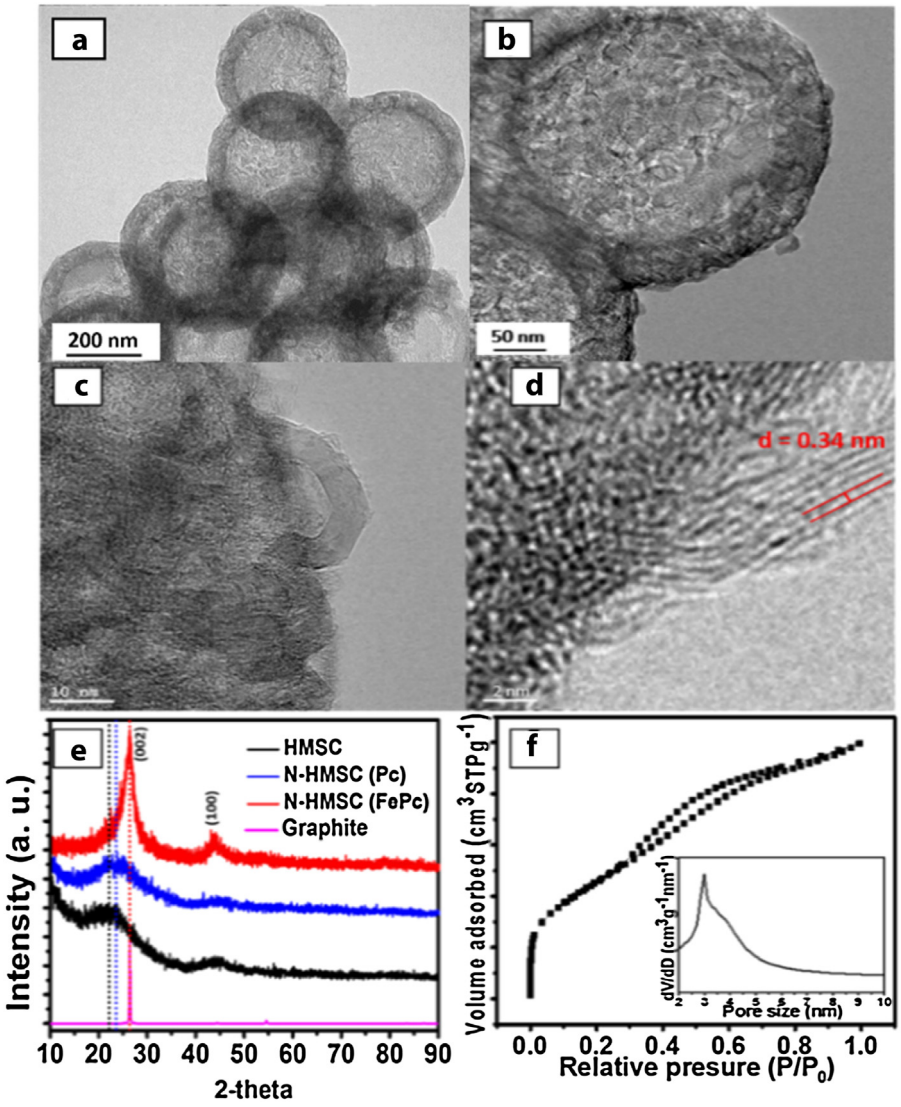

Fig. 1. (a-d) HR-TEM images of N-HMSC (FePc) at different magnifications and (e) XRD patterns of different samples. (f) Nitrogen sorption isotherms of N-HMSC (FePc) with corresponding pore-size distribution (inset).

source, further clearly proving our argument on catalytic activity of Fe on the formation of graphitic phases.

The crystal structure of the prepared catalysts was further evaluated using X-ray diffraction (XRD) (Fig. 1(e)). All the catalysts show two broad signals, which correspond to (002) and (110) phases (JCPDS card No. 41-1487) typical of turbostratic carbon. No other signal for Fe species is seen in N-HMSC (FePc). Interestingly, Fe/N-HMSC (FePc) shows several sharp peaks corresponding to Fe_3O_4 and Fe particles in addition to turbostratic carbon signals (Fig. S4 of SI), clearly indicating the presence of Fe species remaining in the carbon framework, which is in agreement with SEM and TEM images (Fig. S2 and S3 of SI). Interestingly, the undoped HMSC shows a (002) peak at 22°, whereas the same (002) peak is shifted and observed at higher angles of 23 and 26° for N-HMSC (Pc) and N-HMSC (FePc), respectively, as shown by dashed lines in Fig. 1e, which are much closer to the (002) peak position of pristine graphite at 26.5°. This increase in the 2-theta value signifies that interlayer distance between graphitic sheets reduces with N-doping and further reduces in the presence of Fe. Furthermore, it is also found from the XRD that the presence of Fe has significant effect on the peak intensity of the samples. In particular, the sharpness of the (002) peak improves in N-HMSC (FePc), hence proving that Fe-treated N-HMSC (FePc) possesses more graphitic structure as compared with HMSC and N-HMSC (Pc). It is also proved that even after Fe leaching, the graphitic nature of the carbon remains intact, which is in good agreement with the observation in the HR-TEM images (Fig. 1(a-d)). The superior graphitic nature of N-HMSC (FePc) was further confirmed by Raman spectroscopy (Fig. S5 of SI). It shows typical D and G bands at 1336 and 1578 cm^{-1}, which are characteristic of the disordered carbon and sp^2 hybridized graphitic carbon, respectively. The decrease in I_D/I_G ratio is observed from 1.01 for HMSC to 0.97 for N-HMSC (FePc), illustrating increasing order and graphitic nature in N-HMSC (FePc).

Fig. 1(f) and Fig. S6 of SI reveal the nitrogen isotherms of all the prepared HMSC samples. It can be noticed that all the HMSC-based catalysts show Type IV isotherms with H4 hysteresis loops ($P/P_o \geq 0.2$), which are typical for mesoporous structures. The surface area calculated by the multipoint Brunauet-Emmett-Teller (BET) method was determined to be 1716.6, 1539.3, 1488.8, and 867.1 $m^2\,g^{-1}$ for HMSC, N-HMSC (Pc), N-HMSC (FePc), and Fe/N-HMSC (FePc), respectively. After removing Fe particles by HF washing, resulting N-HMSC (FePc) possesses higher surface area and pore volume compared with Fe/ N-HMSC (FePc), almost similar to those of N-HMSC (Pc). However, the mesopore volume and

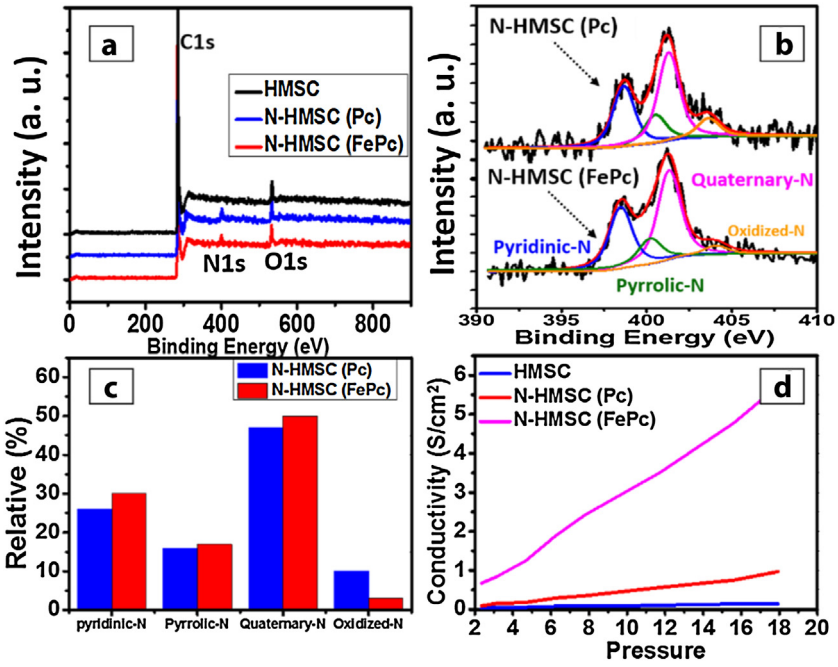

Fig. 2. (a) XPS survey spectra of prepared samples. (b) High-resolution N 1s XPS spectra and (c) relative percentage of N species in N-HMSC (Pc) and N-HMSC (FePc). (d) Variation in electrical conductivity for samples under different pressures.

pore size of N-HMSC (FePc) are found to be higher than those of N-HMSC (Pc), which can be attributed to the removal of Fe particles. Table S1 of ESI† shows the detailed surface parameters for various HMSC materials.

To study the chemical composition and the effect of doping, X-ray photoelectron spectroscopic (XPS) measurements were carried out (Fig. 2(a)). Typical C, O and N peaks are found in all the samples except HMSC, which clearly indicates that the N atoms were successfully incorporated into the carbon structure in N-HMSC (Pc) and N-HMSC (FePc). As expected, no Fe peak is observed in XPS peak survey for N-HMSC (FePc), which clearly reveals the complete removal of Fe during HF washing. The N contents are found to be almost identical with 4.33 and 4.04 at% for N-HMSC (Pc) and N-HMSC (FePc), respectively, indicating Fe has almost no effect on N doping in the carbon framework (Table S2 of SI). As expected, Fe was found to be present in Fe/N-HMSC (FePc) structure as shown in XPS spectrum (Fig. S7 of SI). The binding configurations of the doped N can be identified by N 1s peak deconvolution (Fig. 2(b)). The N atoms are found to be bonded to the surrounding C atoms in the forms of pyridinic, pyrrolic, quaternary, and pyridinic oxidized-N with the binding energy of 398.5, 400.6, 401.5, and 403.5 eV, respectively [43,44]. As shown in Fig. 2(b), the atomic percentage of pyridinic-N and quaternary-N is found to be higher in N-HMSC (FePc) as compared with N-HMSC (Pc), whereas oxidized-N, known to be electrochemically inactive, is observed much lower for N-HMSC (FePc). The concentration and type of N doping are found to be almost similar for Fe/N-HMSC (FePc) and N-HMSC (FePc), indicating negligible influence of Fe on N species (Fig. S7(a) of SI).

Since pyridinic and pyrrolic N have lone pair of electrons, they can donate their electrons to carbon π conjugation system and consequently reduce the band gap of the resultant doped carbon [45]. Therefore, the nitrogen species can have a profound effect on enhancing the electrical conductivity of the doped carbon. It is found that the N-HMSC (Pc) shows better conductivity than HMSC due to the presence of lone pair of electrons on the bonded N atom (Fig. 2(d) and Fig. S8 of SI). As expected, N-HMSC (FePc) outperforms all the other samples in terms of electrical conductivity not only due to the presence of higher amount of pyridinic-N, pyrrolic-N, and quaternary-N species, but also due to higher graphitization of this sample by Fe during carbonization (Fig. 1(d)). This increase in the electrical conductivity, can further facilitate the fast charge transport and is considered to be greatly beneficial for the OER [46,47].

The electrocatalytic activity towards OER was investigated by using a standard three-electrode system. Fig. 3(a) and (b) show the polarization curves for OER and Tafel slopes at a slow scan rate of 5 mV s^{-1}. The potential required for water oxidation to obtain current density of 10 mA cm^{-2} is commonly used to judge the OER activity in research community, which is a metric relevant to solar fuel synthesis [22,48]. As shown in Fig. 3(a) and Table S3, the N-HMSC (FePc) generated the 10 mA cm^{-2} of OER current density at a potential of 0.75 V (1.72 V vs. RHE.) with a low overpotential (η) of only 0.49 V, which is much lower than those of other HMSC catalysts, VC, and Pt/C.

N-HMSC (Pc) also illustrates better performance than bare HMSC, VC, and Pt/C. These results suggest that doped N has significant effect on OER and functions as active catalytic sites during the OER process [30,49]. The pyridinic N is present at the edge of the graphitic sheet, and thus it can share one lone pair of electrons with the neighbouring carbon atom, on which electrochemical adsorption of OH^- is favored, and can be considered as an active sites. On the other hand, quaternary-N can influence the electroneutrality of surrounding carbon by high electronegativity of N, and as a consequence, the adsorption of OH^- on these electropositive carbon increases [17,49]. Furthermore, on comparing the OER activity of Fe-free N-HMSC (FePc) and Fe/N-HMSC (FePc), it is found that the former shows almost the same or slightly better OER activity than the latter, suggesting that physical presence of Fe may not be necessary for OER. N is necessary for OER as an active part, but Fe may not takes part in the OER. This is a first report on the role and necessity of Fe in Fe-N-C system for OER although similar conclusions were reported by a few earlier works for ORR [50–53]. However, this result can be surprising in the light of the several other works reporting Fe-N-C as active center for ORR [54,55]. Although Fe does not contribute significantly to ORR as an active center, as can be inferred from the much improved activity of N-HMSC (FePc), the

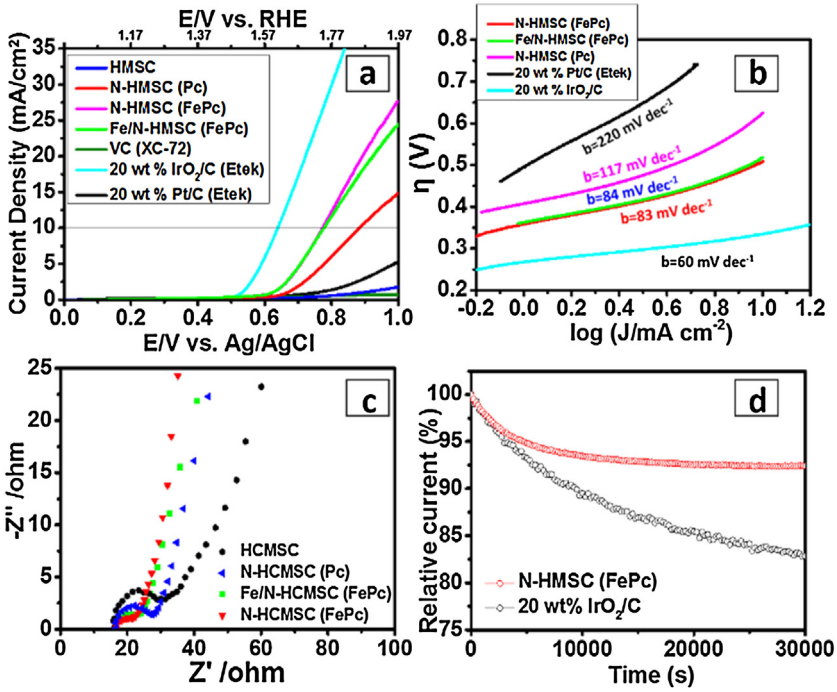

Fig. 3. (a) LSV curves for OER currents of prepared catalysts in 0.1 M KOH solution with 1600 rpm at a scan rate of 5 mV S^{-1}. (b) Tafel plots of OER currents in (a). (c) Nyquist plots of different samples. (d) Chronoamperometric response at a constant potential at 10 mA cm^{-2} of N-HMSC (FePc) and 20 wt% IrO_2/C.

presence of Fe is very important for the preparation of high efficient graphitized N-doped carbon OER electrochemical catalyst.

The OER kinetics of the above catalysts are studied by Tafel plots (Fig. 3(b)). The resulting Tafel slopes are found to be ~60, ~83, ~84, ~117, and ~220 mV dec^{-1} for 20 wt% IrO_2/C, N-HMSC (FePc), Fe/N-HMSC (FePc), N-HMSC (PC), and 20 wt% Pt/C, respectively. (Table S3 of SI). Hence, it can be also surmised that physical presence of Fe is not necessary for OER. Furthermore, since most Fe species in Fe/N-HMSC are found to be embedded with surrounding graphite-like carbon structure, the Fe species are blocked from interacting with OH^-, and thus, it is unlikely that the Fe sites are active centers for OER. To evaluate the variation in OER activity in the presence of Fe in N-HMSC (FePc), we have altered the washing time of N-HMSC (FePc) from 24 h to 5 h. As seen in Fig. S9a of ESI†, clearly upon reducing the washing time, XPS shows the presence of 0.45% of Fe for N-HMSC (FePc) washed for 5 h, which was absent in N-HMSC (FePc) washed for 24 h. However, ORR activity for both the samples is found to be almost the same again as can be seen in Fig. S9(b) of SI The results show that the physical presence of Fe in our N-HMSC (FePc) samples is not a critical factor which influences the OER activity.

To further evaluate the efficiency of the catalytic reaction of various prepared catalysts, we also investigated the catalytic kinetics by electrical impedance spectroscopy (EIS) (Fig. 3(c)). Nyquist plots based on EIS analysis exhibit a much smaller charge-transfer resistance for N-HMSC (FePc), which clearly indicates its better electronic transport capability. Therefore, it can be surmised that due to the high surface area and better conductivity, N-HMSC (FePc) undoubtedly facilitates faster charge transfer, causing smaller Tafel slope and enhanced OER performance. Although the present OER performance of N-HMSC (FePc) is not as good as 20 wt.% IrO_2/C and reported Ir or Ru-based materials (Table S3 of SI), the former has wide scope to be improved further and can be more stable and economically beneficial compared to the latter materials [22,45]. The stability of N-HMSC (FePc) for the OER was also examined with chronoamperometric method and was compared with that of IrO_2/C (20 wt.%). Compared with 17% decrease for IrO_2/C, only a decrease of 7.5% in the OER current, at constant potentials (1.60 V for IrO_2 and 1.72 V for N-HMSC (FePc) at 10 mA cm^{-2}) over 30000 s of continuous operation, was found in N-HMSC (FePc). The higher stability of N-HMSC (FePc) is ascribed to the stable covalent C—N bonds in the carbon framework, suggesting that the active sites in the carbon do not suffer from significant activity degradation after long-term usage, whereas IrO_2/C suffers from agglomeration that causes a reduction in stability [6,11]. This clearly suggests that the N-HMSC (FePc) is a highly competent OER catalyst with the reasonably high performance and stability.

4. Conclusions

In summary, a novel core-shell highly graphitized N-HMSC (FePc) with large surface area was synthesized for the first time through nanocasting using FePc as a single precursor for N, Fe, and carbon, and tested as an OER catalyst. To study the necessity and effect of Fe on the catalyst preparation and electrocatalytic OER activity, different modes of preparation of techniques were adopted. Interestingly, unlike the several earlier works reporting Fe-N-C as active center for ORR, it was found that the physical presence of Fe does not play any significant role in OER although the presence of N is undoubtedly needed for efficient catalysis. Furthermore, on comparing the activity of N-HMSC (Pc) and N-HMSC (FePc), it can be concluded that Fe helps to increase more effective N species with high edge exposure and graphiticity in the N-HMSC framework, which eventually generate the highly efficient N-doped carbon catalyst for OER. Therefore, the current work provides more on new fundamental insight into catalytic phenomenon, which is of great significance for better understanding and designing the catalysis. While it has been found that Fe-free N-doped carbon prepared in the presence of Fe is highly active for OER, we have not ruled out the possibility that tiny amount of Fe, which may exist beyond the spectroscopic detection limit can also contribute to the activity in parallel mechanism. Eventually, this will open a new direction for the preparation of efficient heteroatom-doped carbon materials and contribute a lot to better understanding of active sites for OER.

High graphitic property, large surface area, nitrogen doping, and unique structure of N-HMSC (FePc) can contribute a lot to its high electrical conductivity, large number of active sites, and excellent stability, eventually leading to highly efficient cost-effective OER electrocatalyst.

Acknowledgments

The work was supported by NRF grant (NRF-2014K2A3A1000240) and Global Frontier R&D Program (NRF-2011-0031571) funded Korean government for financial support. Authors also thank KBSI at Jeonju and Pusan for TEM, HR-TEM and XPS measurements. This study was also supported by the Swedish Foundation for International Cooperation in Research and Higher Education (STINT).

Appendix A. Supplementary data

Supplementary data associated with this article can be found, in the online version, at http://dx.doi.org/10.1016/j.apcatb.2016.03.031.

References

[1] M. Armand, J.-M. Tarascon, Nature 451 (2008) 652–657.
[2] M.G. Walter, E.L. Warren, J.R. Mckone, S.W. Boettcher, Q. Mi, E.A. Santori, N.S. Lewis, Chem. Rev. 110 (2010) 6446–6473.
[3] Z. Jintao, Z. Zhenghang, X. Zhenhai, D. Liming, Nat. Nanotechnol. 48 (2015) 444–452.
[4] N. Jiang, B. You, M. Sheng, Y. Sun, Angew. Chem. Int. Ed. 54 (2015) 6251–6254.
[5] X. Long, J. Li, S. Xiao, K. Yan, Z. Wang, H. Chen, S. Yang, Angew. Chem. Int. Ed. 53 (2014) 7584–7588.
[6] F.-D. Kong, S. Zhang, G.-P. Yin, J. Liu, Z.-Q. Xu, Int. J. Hydrogen Energy 38 (2013) 9217–9222.
[7] Y. Gorlin, T.F. Jaramillo, J. Am. Chem. Soc. 132 (2010) 13612–13614.
[8] J. Masa, W. Xia, I. Sinev, A. Zhao, Z. Sun, S. Grutzke, P. Weide, M. Muhler, M.W. Schuhmann, Angew. Chem. Int. Ed. 53 (2014) 8508–8512.
[9] S. Siracusano, N. Van Dijk, E. Payne-Johanson, V. Baglio, A.S. Aricò, Appl. Catal. B: Environ. 164 (2015) 488–495.
[10] J. Suntivich, K.J. May, H.A. Gasteiger, J.B. Goodenough, S.-H. Yang, Science 334 (2011) 1383–1385.
[11] X. Yu, M. Zhang, W. Yuan, G. Shi, J. Mater. Chem. A 3 (2015) 6921–6928.
[12] L. Trotochaud, J.K. Ranney, K.N. Williams, S.W. Boettcher, J. Am. Chem. Soc. 134 (2012) 17253–17261.
[13] Z. Lu, W. Xu, W. Zhu, Q. Yang, X. Lei, J. Liu, Y. Li, X. Sun, X. Duan, Chem. Commun. 50 (2014) 6479–6482.
[14] J. Wang, K. Li, H.-X. Zhong, D. Xu, Z. -l. Wang, Z. Jiang, Z.-J. Wu, X.-B. Zhang, Angew. Chem. Int 54 (2015) 10530–10534.
[15] D.U. Lee, B.J. Kim, Z. Chen, J. Mater. Chem. A 1 (2013) 4754–4762.
[16] C. Domínguez, F.J. Pèrez-Alonso, M.A. Salam, S.A. Al-Thabaiti, M.A. Peña, F.J. García-García, L. Barrio, S. Rojas, Appl. Catal. B: Environ. 183 (2016) 185–196.
[17] Y. Zhao, R. Nakamura, K. Kamiya, S. Nakanishi, K. Hashimoto, Nat. Commun. 4 (2013) 2390–2397.
[18] F. Razmjooie, K.P. Singh, J.-S. Yu, Catal. Today 260 (2016) 148–157.
[19] F. Razmjooei, K.P. Singh, M.Y. Song, J.-S. Yu, Carbon 78 (2014) 257–267.
[20] S. Chen, J. Duan, M. Jaroniec, S.-Z. Qiao, Adv. Mater. 26 (2014) 2925–2930.
[21] R. Li, Z. Wei, X. Gou, ACS Catal. 5 (2015) 4133–4142.
[22] L. Wang, F. Yin, C. Yao, Inter int, J. Hydrogen Energy. 39 (2014) 15913–15919.
[23] Z. Lin, G.H. Waller, T. Liu, M. Liu, C.-P. Wong, Carbon 53 (2013) 130–136.
[24] K.P. Singh, E.J. Bae, J.-S. Yu, J. Am. Chem. Soc. 137 (2015) 3165–3168.
[25] Y. Zhang, W.-J. Jiang, L. Guo, X. Zhang, J.-S. Hu, Z. Wei, L.-J. Wan, ACS Appl. Mater. Interfaces 7 (2015) 11508–11515.
[26] M. Lefèvre, E. Proietti, J.-P. Jaouen Dodelet, Science 324 (2009) 71–74.
[27] F. Razmjooei, K.P. Singh, E.J. Bae, J.-S. Yu, J. Mater. Chem. A 3 (2015) 11031–11039.
[28] N.I. Andersen, A. Serov, P. Atanassov, Appl. Catal. B: Environ. 163 (2015) 623–627.
[29] Y. Su, Y. Zhu, H. Jiang, J. Shen, X. Yang, W. Zou, J. Chen, C. Li, Nanoscale 6 (2014) 15080–15089.
[30] J.-L. Shui, N.K. Karan, M. Balasubramanian, S.-Y. Li, D.-J. Liu, J. Am. Chem. Soc. 134 (2012) 16654–16661.
[31] Y. Zhao, K. Kamiya, K. Hashimoto, S. Nakanishi, J. Phys. Chem. C 119 (2015) 2583–2588.
[32] R.A. Rincon, J. Masa, S. Mehrpour, F. Tietz, W. Schuhmann, Chem. Commun. 50 (2014) 14760–14762.
[33] P. Gandian, M. Prabu, J. Sanetuntikul, S. Shanmugam, ACS Catal. 5 (2015) 3625–3637.
[34] P. Li, Z. Jin, D. Xiao, J. Mater. Chem. A 2 (2014) 18420–18427.
[35] J. Wang, D. Gao, G. Wang, S. Miao, H. Wu, J. Li, X. Bao, J. Mater. Chem. A 2 (2014) 20067–20074.
[36] H. Peng, Z. Mo, S. Liao, H. Liang, L. Yang, F. Luo, H. Song, Y. Zhong, Sci. Rep. 3 (2013) 1810.
[37] H.W. Liang, W. Wei, Z.S. Wu, X. Feng, K. Mullen, J. Am. Chem. Soc. 135 (2013) 16002–16005.
[38] M. Zhou, C. Yang, K.-Y. Chan, Adv. Energy. Mater. 4 (2014) 1400840–1400845.
[39] D.-S. Yang, M.Y. Song, K.P. Singh, J.-S. Yu, Chem. Comm. 15 (2015) 2450–2453.
[40] D. Bhattacharjya, M.-S. Kim, T.-S. Bae, J.-S. Yu, J. Power Sources 244 (2013) 799–805.
[41] K.P. Singh, M.Y. Song, J.-S. Yu, J. Mater. Chem. A 2 (2014) 18115–18124.
[42] D.-S. Yang, D. Bhattacharjya, M.Y. Song, J.-S. Yu, Carbon 67 (2014) 736–743.
[43] N.K. Chaudhari, M.Y. Song, J.-S. Yu, Sci. Rep. 4 (2014) 5221.
[44] K. Chaudhari, M.Y. Song, J.-S. Yu, Small 10 (2014) 2625–2636.
[45] P. Wu, Y. Qian, P. Du, H. Zhang, C. Cai, J. Mater. Chem. 22 (2012) 6402–6412.
[46] D.-S. Yang, S. Chaudhari, K.P. Rajesh, J.-S. Yu, ChemCatChem 6 (2014) 1236–1244.
[47] D.-S. Yang, D. Bhattacharjya, M.Y. Song, F. Razmjooei, Q.-H. Yang, J. Ko, J.-S. Yu, ChemCatChem 7 (2015) 2882–2890.
[48] Y. Liang, Y. Li, H. Wang, J. Zhou, J. Wang, T. Regier, H. Dai, Nat. Mater. 10 (2011) 780–786.
[49] M. Li, L. Zhang, Q. Xu, J. Niu, Z. Xia, J. Catal. 314 (2014) 66–72.
[50] E.J. Biddinger, S. Ozkan, J. Phys. Chem. C 114 (2010) 15306–15314.
[51] K.H. Lim, H. Kim, Appl. Catal. B: Environ. 158–159 (2014) 355–360.
[52] D. Deng, L. Yu, X. Chen, G. Wang, L. Jin, X. Pan, J. Deng, G. Sun, X. Bao, Angew. Chem. Int. 52 (2013) 371–375.
[53] G. Liu, X. Li, P. Ganesan, B.N. Popov, Electrochim. Acta 55 (2010) 2853–2858.
[54] S. Chen, J. Duan, J. Ran, M. Jaroniec, S.Z. Qiao, Energy Environ. Sci. 6 (2013) 3639–3699.
[55] H. Chung, J.H. Won, P. Zelenay, Nat. Commun. 4 (2013) 1922.